Electronic Supplementary Information

Observation and Mechanism of Cryo N₂ Cleavage by a Tantalum Cluster

Daniela V. Fries, Matthias P. Klein, Annika Steiner, Marc H. Prosenc and Gereon Niedner-Schatteburg

Fachbereich Chemie and Forschungszentrum OPTIMAS,
Technische Universität Kaiserslautern, 67663 Kaiserslautern, Germany

Text 1: Detailed Experimental and Computational Methods

The experiments were performed with a customized Fourier transform ion cyclotron resonance (FT-ICR) mass spectrometer (Apex Ultra, Bruker Daltonics). This specific apparatus configuration allows us to generate cluster ions and isolate required mass complexes. Furthermore, we are able to adsorb reaction gases while trapping the ions in the hexapole cell and record mass spectra of the adsorbate complexes. Finally, we can examine the ions in the ICR cell by adsorption kinetics and infrared (multi) photon dissociation (IR-PD) spectroscopy.

First, we generate required cluster ions using a home-built laser vaporization (LVAP) source as described before.[1,2] The second harmonic of a pulsed Nd:YAG laser (Spitlight300, Innolas, 20 Hz) was used to evaporate tantalum atoms from a rotating tantalum foil (0.5 mm thick. 99.95 %. Alfa Aesar). Next, a gas pulse created from a piezoelectric valve[3] captures the hot plasma. While guided subsequently through the expansion channel (69 mm long, 2 mm diameter) the atoms and ions cool down and aggregate. Passing electrostatic lenses, the resulting cluster size distribution reaches the 90° ion beam bender. The bare clusters can be mass selected by a quadrupole mass filter and reach the cryogenic hexapole cell (10 K) subsequently. Therein, we are able to trap required mass complexes and introduce buffer or reaction gases. This can be done continuously or in pulses. For our investigations on tantalum clusters we only used continuously injection of up to $2.6 \cdot 10^{-7}$ mbar N_2. To achieve sufficient cluster signal and thermalization, additional collision gas (He; up to $6.8 \cdot 10^{-6}$ mbar) was introduced into the hexapole. After trapping the clusters and cluster adsorbates for various storage times (0 - 20 s), the ions are guided by electrostatic lenses into the FT-ICR cell for detection. If required, it is possible to isolate ion complexes within and introduce further reaction gas into this infinity cell.[4]

Reaction delay scans were recorded in order to investigate adsorption kinetics of nitrogen molecules to tantalum clusters. From this, we obtain a temporal evolution of mass spectra, which is evaluated by the program DataAnalysis 4.0 (Bruker Daltonics). The outcoming signal intensities and assigned storage times of each adsorbate complexes are input data for evaluation by evofit [5]. This program performs pseudo-first-order fits, from which we receive relative rate constants for adsorption ($k_{(n,m)}$) and desorption steps ($k_{-(n,m+1)}$), respectively.

$$[Ta_n(N_2)_m]^+ + N_2 \qquad [Ta_n(N_2)_{m+1}]^+ \qquad \underset{k_{-(n,m+1)}}{\overset{k_{(n,m)}}{\rightleftharpoons}}$$
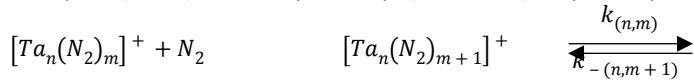
The relative rate constants ($k_{(n,m)},\ k_{-(n,m+1)}$) determine the absolute rate constants ($k_{(n,m)}^{abs}, k_{-(n,m+1)}^{abs}$), the absolute collision gas number densities $\rho_{N_2}(T)$ serving as the conversion factor.

$$k_{(n,m)}^{abs} = \frac{k_{(n,m)}}{\rho_{N_2}(T)} \qquad k_{-(n,m+1)}^{abs} = \frac{k_{-(n,m+1)}}{\rho_{N_2}(T)}$$

Approximate values for $\rho_{N_2}(T)$ are indirectly given by the pressure in the surrounding chamber p_c^{300K} and an effective geometry factor c_{app}.

$$\rho_{N_2}(T) = \frac{c_{app} \cdot p_c^{300K}}{k_B \cdot T_{300K}}$$

This geometry factor c_{app} shows a significant dependency on the temperature of the hexapole ion trap. We evaluated this factor to 1.8 at 26 K (uncertainty of ± 50 %) by numerous of previous kinetic studies of transition metal cluster cations with neutral reactants at cryo temperatures. Three models are used for determination of collision rates. The average dipole orientation (ADO) theory is based on a concept of a classical trajectory of a linear dipole in the field of a point charge.

$$k_{coll} = \frac{q}{2\varepsilon_0\sqrt{\mu}} \cdot \left(\sqrt{\alpha} + c\mu_D \sqrt{\frac{2}{\pi k_B T}}\right)$$

Whereby μ is the reduced mass of the cluster adsorbate complex, μ_D stands for the dipole moment and α is the polarizability. The parameter c can take values from 0 to 1 and can be expressed by the polarizability of the neutral reactant, here N_2. The volume α' and μ_D.[6] It simplifies to the Langevin rate in the case of a negligible dipole moment. The ADO theory often underestimates the reaction rates for charged clusters with small molecules. Nevertheless, it is frequently used to calculate reaction rates for charged clusters with small molecules.[7] Therefore, Kummerlöwe and Beyer[8] devised two new models to determine collision rates of ionic clusters with neutral molecules. While the hard sphere average dipole orientation (HSA) model assumes a point charge in the center of the ionic cluster, the charge in the surface charge capture (SSC) theory is able to migrate to the cluster surface by its attractive interaction with the neural collision partner.

For performing IR-PD experiments, a tunable IR laser (δt = 7 ns) is coupled into the ICR cell. This laser is comprised of a KTP/KTA optical parametric oscillator/amplifier (OPO/OPA. LaserVision) system pumped by a pulsed injection seeded Nd:YAG laser (10 Hz, PL8000, Continuum). To obtain IR radiation (1100 – 2400 cm^{-1}), an $AgGaSe_2$ crystal is used to generate the difference frequency (DF) between the OPA signal and idler waves. During irradiation with the IR laser, the ions are isolated and trapped in the ICR cell. Subsequently, every ion package is treated by 7 – 10 laser pulses (0.3 – 4.0 mJ/pulse) to yield sufficient fragment ions. A series of fragmentation mass spectra is recorded while continuously scanning the IR wavelength.

$$\sum_I F_I \Big/ \left(\sum_I F_I + \sum_I P_I\right)$$

The measured IR-PD signal is evaluated as , where F_I and P_I represent fragment and parent ion signal, respectively. Finally, the determined fragmentation efficiency is plotted as a function of laser frequency in order to obtain an IR-PD spectrum.

All quantum chemical calculations are carried out by the program package Gaussian 09[9] and the Gaussian 16 suite[10]. We employed the PBE0 functional[11, 12] for nonlocal corrections and the def2-TZVP basis set[13, 14] for all atoms. We did so in continuation previous studies which have succeeded to model N_2 adsorption before, as e.g. in the cases of Rhodium clusters [15] and Nickel clusters [16, 17]. We did so in continuation of previous studies which have succeeded to model N_2 adsorption before, as e.g. in the cases of Rhodium clusters [15] and Nickel clusters [16, 17]. Moreover, we verified our choice of method by employing a multitude of available exchange correlation functionals, and CC2 calculations on top (cf. Fig. S8) along some part of the reaction path of initial N_2 activation along three local minima ($I2_{(4,1)}$ and $I3_{(4,1)}$ and $P_{vic(4,1)}$) and both intermediate transition states ($TS23_{(4,1)}$ and $TS3P_{vic(4,1)}$). It shows that the optimized minimum structures and transition states are robust (for a survey of some critical geometric parameters refer to Table S15 in the supplement), as well as the relative energies by less than 30 kJ/mol (cf. Table S14). We take this as a valid gauge of the chosen level of theory, PBE0/def2-TZVP. All stationary states were checked by second derivative calculations revealing no (minima) and only one (transition state) imaginary frequency. Reaction paths were searched by QST2/3[18] or linear transit methods[19] and after location and optimization of the transition states scanned by IRC calculations.[20] Orbital analyses were performed using Molecular Orbitals as well as Natural Bonding Orbitals as employed in the Gaussian 16 program.[21, 22]

Text 2: Nomenclature for the Ta_4^+ cluster and its adsorbates

There are 14 complexes of the form $[Ta_4(N_2)_m]^+$, where m stands for the number of N_2 molecules attached to the cluster. The index m ranges from 0 to 13. For ease of reference, we use the notation $(4,m)$. The 14 complexes are interlinked by 13 processes, respectively, in the form of adsorption and desorption reactions. The rate constants for these adsorption and desorption processes are labelled as k_m and $k_{-(m+1)}$. Therefore, m can assume values from 0 to 12.

We use e.g. $k_0 := k_{0\to 1}$ for the adsorption step:

$$Ta_4^+ + N_2 \to \left[Ta_4(N_2)_1\right]^+$$
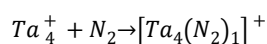
and $k_{-1} := k_{1\to 0}$ for the desorption step:

$$\left[Ta_4(N_2)_1\right]^+ \to Ta_4^+ + N_2.$$
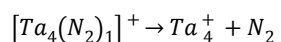
To simplify the description of the products, we use the following subscript abbrevations for the relative positions of the resulting nitride ligands: gem (geminal, on the same Ta-Ta edge), vic (vicinal, on neighbored Ta-Ta edges), and dis (distal, on opposite edges of the Ta_4^+ tetrahedron).

Text 3: Detailed discussion of the intermediate $I1_{(4,1)}$

According to an NBO analysis, there are minor contributions from $6s$ and $6p$ orbitals which we omit in further discussion. The Ta1 atom provides for five $5d$ electrons. It utilizes three of these to form three σ-bonds to the remaining three Ta atoms of the cluster. The Ta1 atom thereby experiences a local weak ML3 ligand field splitting of the $5d$ orbitals which destabilizes the thus empty d_{z^2} orbital.[23] The remaining two d electrons fill the d_{xz} orbital. This d_{xz} orbital is a lone pair orbital at the Ta1 atom within the NBO framework. The N_2 ligand's lone pair donates towards the empty d_{z^2} orbital which locates perpendicular to the (Ta1 Ta2 Ta3) plane. The bonding of the N_2 ligand to the Ta1 atom seems to increase the Ta1-Ta4 bond length from 2.52 Å in Ta_4^+ to 2.72 Å in $I1_{(4,1)}$, and the N_2 binding energy amounts to 66 kJ/mol (in the doublet state).

### Text 4: Detailed discussion of the intermediate $I2_{(4,1)}$

The stabilization of $I2_{(4,1)}$ with respect to $I1_{(4,1)}$ is accompanied by a reduction of d(Ta1-N1) to 2.02 Å (-0.11 Å with respect to $I1_{(4,1)}$), an elongation of d(N1-N2) to 1.19 Å (+0.08 Å), and a tilting of the N_2 ligand towards Ta2. The result is a bridged μ_2-κN1:κN1κN2 structure with d(Ta2-N1) = 2.12 Å (-1.00 Å with respect to I1(4,1)) and d(Ta2-N2) = 2.18 Å (-1.80 Å). Note, that this coordination motif corresponds to a tantalum complex with a bridging N_2 unit that is coordinated both side on and end on[23, 24]. Related complexes with I2 type bonding motifs were reported for Gd[25], Sc[26], and V[27]. By the tilting, the distance d(Ta1-Ta4) in $I2_{(4,1)}$ decreases to 2.56 Å (-0.16 Å with respect to $I1_{(4,1)}$) due to the diminished donation of the coordinating nitrogen lone pair electron density into the Ta1 T4 σ*-antibonding orbital. In effect, the Ta1-Ta4 bond strengthens and the distance between the Ta atoms shrinks. Note, that at this point there are no Ta3-N1 and Ta3-N2 interactions.

### Text 5: Detailed discussion of the intermediate $I3_{(4,1)}$

The structure of $I3_{(4,1)}$ reveals the bridged μ_3-κN1:κN1,N2:κN1,N2 bonded nitrogen ligand which comprises an elongated N1-N2 bond of 1.43 Å (+0.24 Å with respect to $I2_{(4,1)}$). The Ta1-N1 distance has decreased to 1.92 Å (-0.10 Å), as well as the Ta2-N2 distances of 2.00 Å (-0.17 Å) and Ta3-N2 distance of 1.96 Å (-2.29 Å). The Ta2-Ta3 bond has elongated from 2.57 Å, $I2_{(4,1)}$, to 2.87 Å, $I3_{(4,1)}$, (+0.30 Å), and the Ta1-Ta3 bond from 2.56 Å, $I2_{(4,1)}$, to 2.92 Å, $I3_{(4,1)}$, (+0.36 Å); the charge density of both bonds dilutes significantly. In parallel, the N1-N2 bond elongates from 1.19 Å, $I2_{(4,1)}$, to 1.43 Å, $I3_{(4,1)}$, (+0.24 Å). Note, that this points to a mere N-N single bond distance as e.g. found in hydrazine[28] and related complexes (1.45 Å). Thus, the adaptive Ta_4^+ cluster enables a bridged μ_3 coordination of N_2 (cf. I3 in Figure 3). The concomitant cleavage of the N_2 triple bond is accompanied by a relaxation of the Ta_4^+ scaffold.

### Text 6: Detailed discussion of the product $P_{vic(4,1)}$

The four Ta N bonds in $P_{vic(4,1)}$ possess almost equal bond length on the order of 1.84 - 1.90 Å. Minor variations might originate from partial double and single bond characters. Accordingly, the two N bridged Ta1-Ta2 and Ta2-Ta3 bonds are equally elongated to 2.81 Å as compared to the non bridged Ta-Ta bonds, e.g. d(Ta1 Ta3) = 2.69 Å.
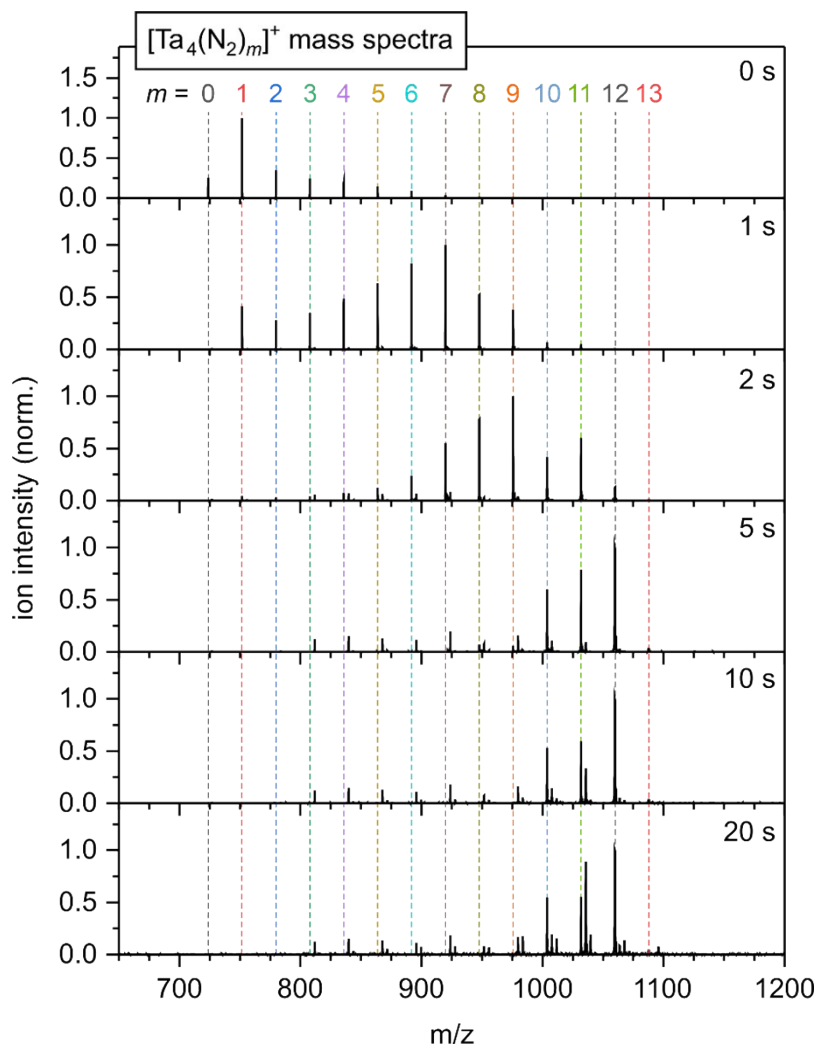
Fig. S1. Temporal evolution of the FT-ICR mass spectra of Ta_4^+ cluster complexes at 26 K and various storage times in the cryogenic hexapole ion trap exposed to an N_2 pressure of $2.6 \cdot 10^{-7}$ mbar. The least quantifiable maximum of N_2 adsorption to Ta_4^+ clusters from the carried-out measurement is 13 N_2.
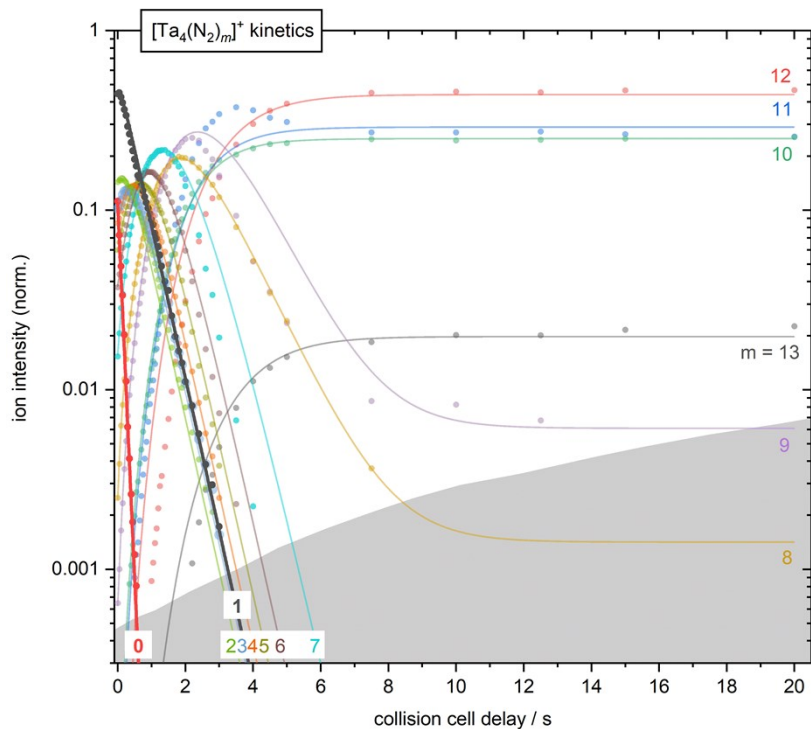
Fig. S2. Isothermal kinetics of N_2 adsorption by mass-selected Ta_4^+ clusters at 26 K, He buffer gas (6.8 · 10^{-6} mbar) and an exposure of 2.6 · 10^{-7} mbar N_2. The experimental data (solid dots) and the fits (solid lines) assume pseudo-first order kinetics for the N_2 adsorption in up to 13 consecutive steps. The kinetics of first and second N_2 adsorption are highlighted. The grey-shaded area indicates the background noise level. Corresponding rate constants of the pseudo-first order fits for each adsorption/desorption is shown in the Supporting Information (cf. Fig. S3)
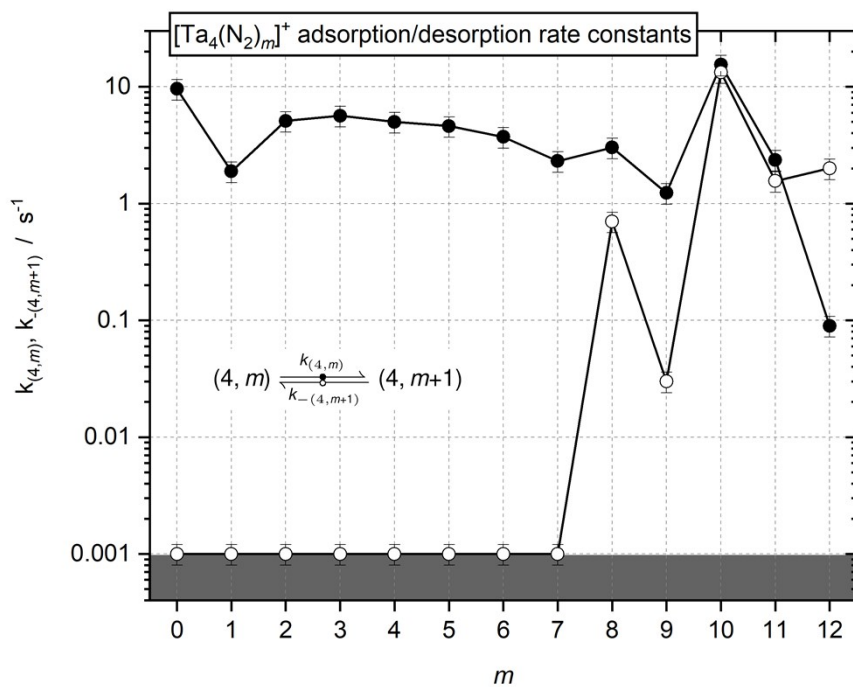
Fig. S3. Observed rate constants resulting from pseudo-first-order fits of measured kinetic data of the Ta_4^+ cluster complex as a function of stepwise N_2 adsorption. Filled circles show the rate of adsorption ($k_{(4,m)}$). Desorption rates ($k_{-(4,m+1)}$) are represented by open circles. The gray shaded area indicates the background noise level.
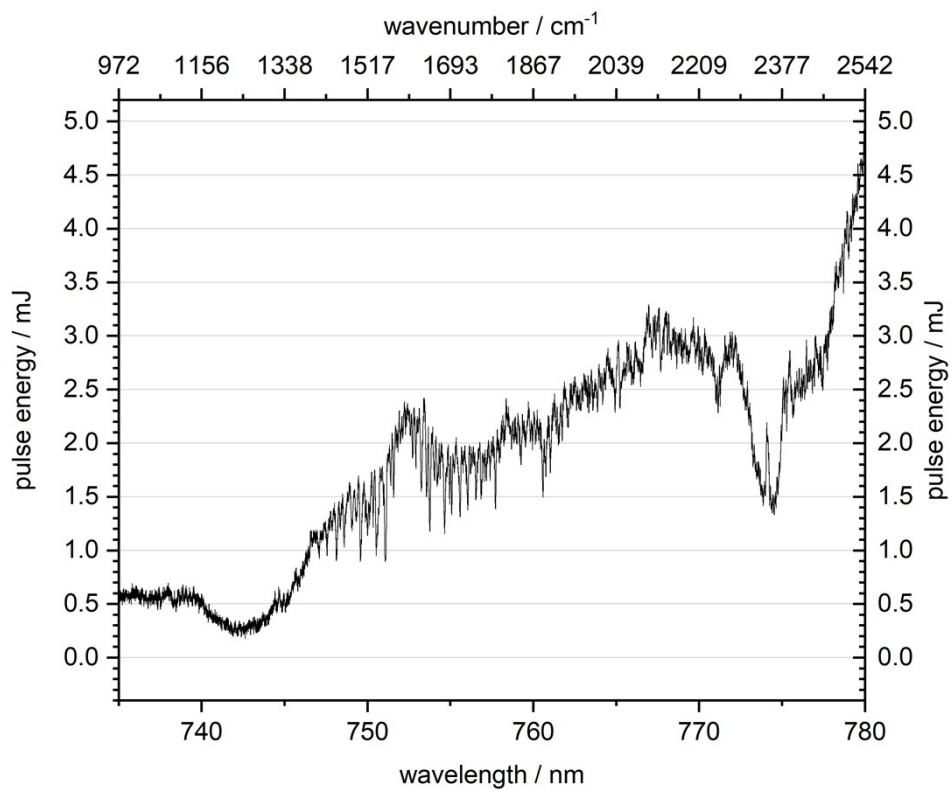
Fig. S4. Laser pulse energy in dependency of wavelength and wavenumber.
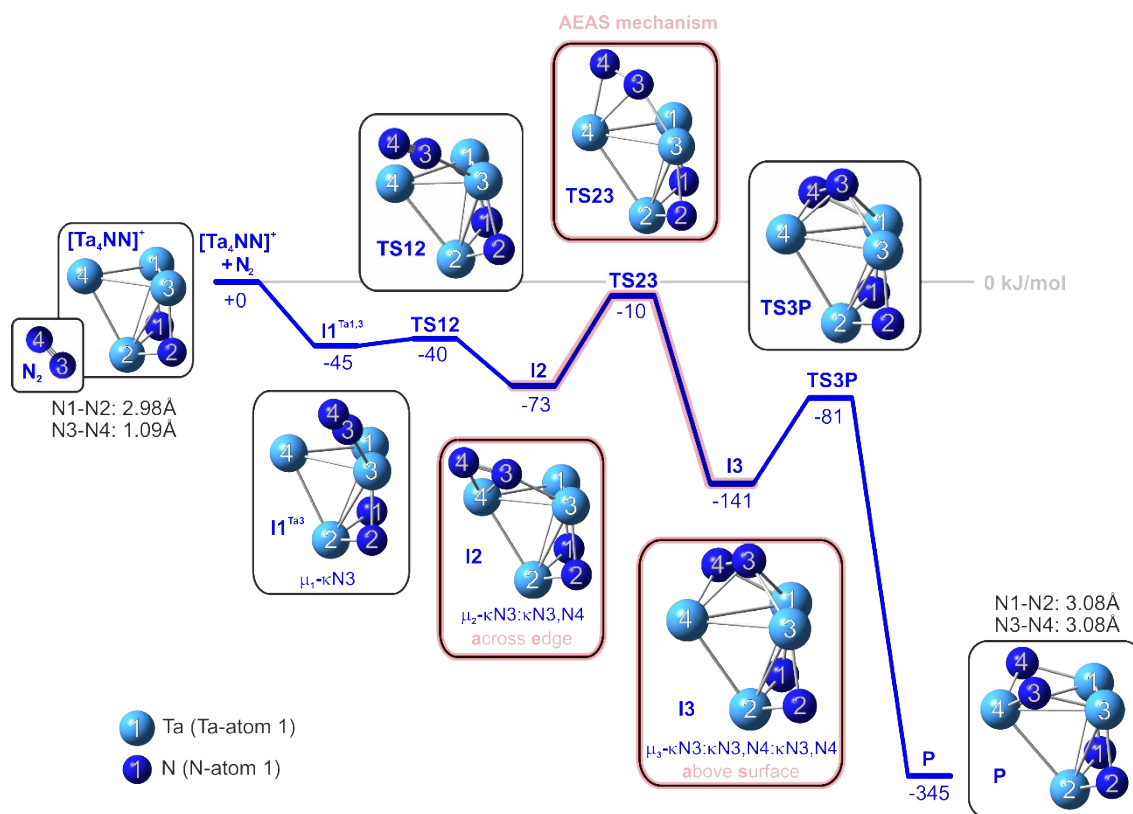
Fig. S5. A reaction pathway of second N_2 cleavage on a $[Ta_4NN]^+$ cluster complex (adsorption site: Ta3). The torsional reorganization of the AEAS mechanism is highlighted. For reasons of clarity, the nomenclature is presented in a shortened form (e.g. here I1 stands for $I1_{(4,2)}$ or rather $I1^{Ta3}_{(4,2)}$).
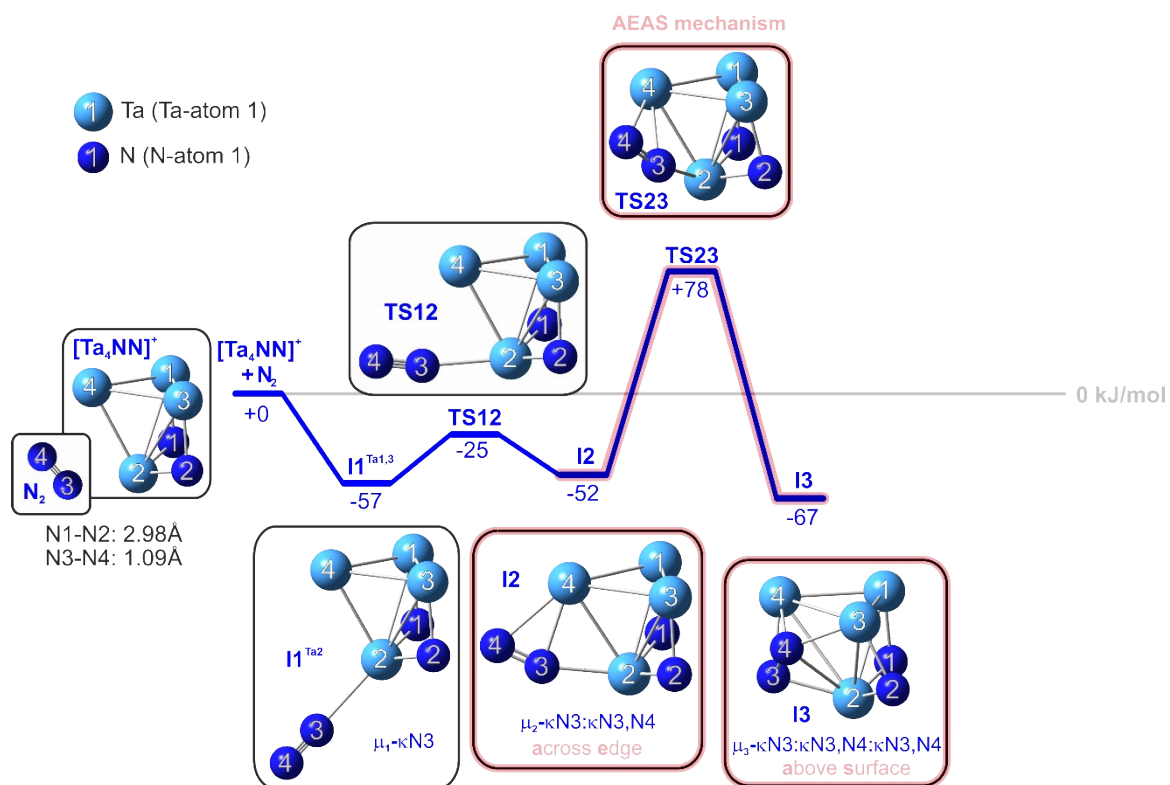
Fig. S6. A reaction pathway of second N_2 cleavage on a $[Ta_4NN]^+$ cluster complex (adsorption site: Ta2). The torsional reorganization of the AEAS mechanism is highlighted. For reasons of clarity, the nomenclature is presented in a shortened form (e.g. here I1 stands for $I1_{(4,2)}$ or rather $I1^{Ta2}_{(4,2)}$).
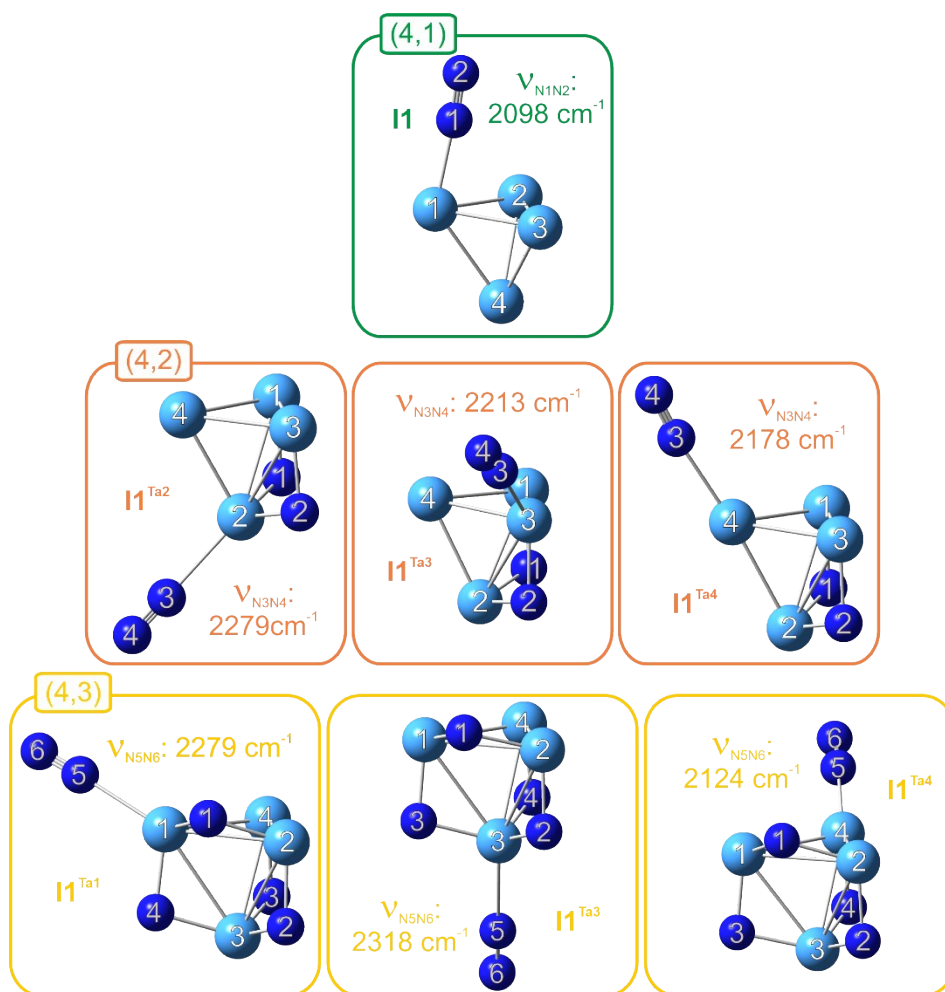
Fig. S7. Model structures with an end on bound N_2 molecule (μ_1-N1 coordination) obtained from DFT calculations on the first, second and third N_2 activation pathway. Their scaled vibrational frequencies are within the range of 2100 cm^{-1} to 2300 cm^{-1} (scale factor: 0.9376).
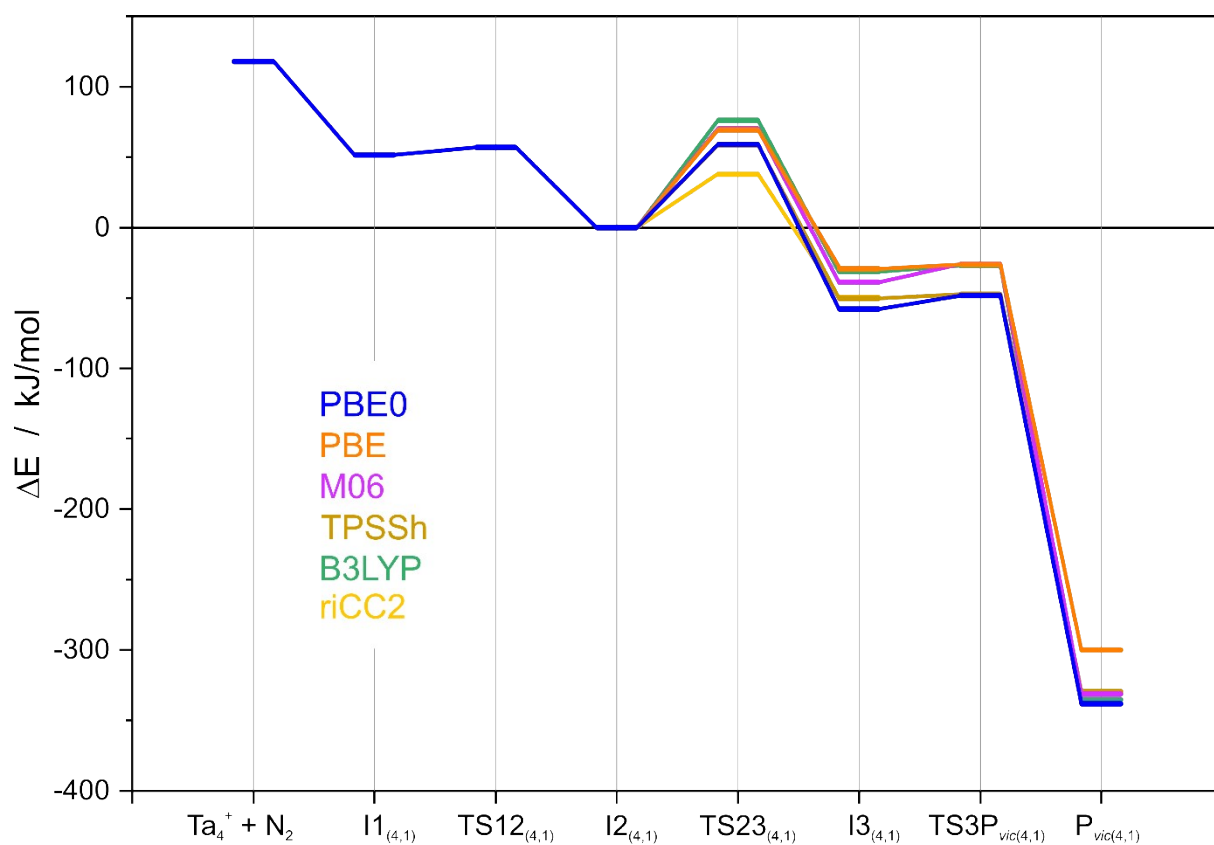
Fig. S8. Reaction path of initial N_2 activation in the case of (n,m)=(4,1) by DFT calculations with a multitude of exchange correlation functionals, and by CC2 calculations. For numerical values refer to Table S14.

Table S1. Relative pseudo-first-order rate constants, absolute rate constants, collision rates and sticking probabilities for the N_2 adsorption on (4,*m*) clusters at a N_2 pressure of $2.6 \cdot 10^{-7}$ mbar. Gray shaded elements highlight sticking probabilities $\gamma > 1$. Orange highlighted values are likely to be questionable as the limits of *evofit* (5) (fit program) have been exceeded.

	$2.6 \cdot 10^{-7}$ mbar N_2			
m	k_{coll} (4,*m*) / 10^{-16} m³/s	$k_{(4,m)}$ / s⁻¹	k_{abs} (4,*m*) / 10^{-16} m³/s	γ
0	6.00	9.58	8.48	1.41
1	6.00	1.88	1.67	0.28
2	5.99	5.10	4.51	0.75
3	5.99	5.65	5.00	0.84
4	5.99	5.01	4.43	0.74
5	5.98	4.60	4.07	0.68
6	5.98	3.72	3.29	0.55
7	5.98	2.31	2.05	0.34
8	5.97	3.02	2.67	0.45
9	5.97	1.23	1.09	0.18
10	5.97	15.43	13.7	2.29
11	5.97	2.37	2.09	0.35
12	5.96	0.09	0.08	0.01

Table S2. Calculated distances in Å of atoms within Ta_4^+, N_2 and $[Ta_4(N_2)_1]^+$ in the doublet state along the activation pathway of the first N_2 molecule on a Ta_4^+ cluster complex.

	$[Ta_4]^+$	N_2	$I1_{(4,1)}$	$TS12_{(4,1)}$	$I2_{(4,1)}$	$TS23_{(4,1)}$	$I3_{(4,1)}$	$TS3P_{(4,1)vic}$	$TS3P_{(4,1)gem}$	$P_{(4,1)vic}$	$TSP_{vic}P_{gem}$	$P_{(4,1)gem}$	$TSP_{vic}P_{dis}$	$P_{(4,1)dis}$
Ta1-Ta2	2.64281		2.53029	2.53803	2.63597	2.58405	2.51053	2.9816	2.58642	2.80981	2.81177	2.54861	2.9854	2.65808
Ta2-Ta3	2.52474		2.54831	2.54441	2.57044	2.4606	2.87221	2.80459	2.9635	2.80852	3.05656	2.84528	2.80194	2.77209
Ta3-Ta4	2.55383		2.52596	2.54142	2.60882	2.51033	2.46294	2.55785	2.61668	2.58246	2.57717	2.5485	2.55304	2.65861
Ta1-Ta4	2.52494		2.72035	2.71223	2.55912	2.58949	2.5635	2.57129	2.46981	2.57679	2.55691	2.67861	2.60097	2.66287
Ta2-Ta4	2.52393		2.52619	2.51859	2.57036	2.77776	2.54261	2.44979	2.61663	2.61516	2.55519	2.54854	2.54783	2.65895
Ta1-Ta3	2.5242		2.53039	2.52825	2.55924	2.59023	2.91928	2.51185	2.58647	2.69019	2.66673	2.54863	2.67202	2.65872
Ta1-N1			2.12606	2.08579	2.0197	2.02836	1.91925	1.91264	2.43664	1.83777	1.85736	1.99248	1.8178	1.85619
Ta1-N2														
Ta2-N1			3.1238	2.51358	2.12104	2.16581	2.19976	2.10592	1.94684	1.89471	1.87219	2.00009	1.94786	
Ta2-N2			3.9722		2.17607	2.10638	2.00254	1.92269	1.96373	1.89543	1.95083	1.99998	1.87395	1.85724
Ta3-N1					3.61223		2.2019	2.29594	1.94692			2.00003		
Ta3-N2					4.24793		1.95998	1.9417	1.96381	1.83664	1.84741	1.99997	1.85766	1.85718
Ta4-N1														1.85593
Ta4-N2												1.99291		
N1-N2		1.08948	1.10833	1.12038	1.18967	1.22901	1.43062	1.66522	1.83186	2.97767		2.71973		4.36624

13

Table S3. Calculated energies of the cluster adsorbate complex $[Ta_4(N_2)_1]^+$ in the doublet and quartet state along the activation pathway of the first N_2 molecule on a Ta_4^+ cluster complex.

	doublet state		quartet state	
	energy E / Ha	ΔE / kJ/mol	energy E / Ha	ΔE / kJ/mol
Ta_4^+, N_2	-337.05023	0	-337.035182	40
$I1_{(4,1)}$	-337.07549	-66	-337.054152	-10
$TS12_{(4,1)}$	-337.07342	-61	-337.050021	1
$I2_{(4,1)}$	-337.09514	-118	-337.074784	-64
$TS23_{(4,1)}$	-337.07269	-59	-337.056313	-16
$I3_{(4,1)}$	-337.11716	-176	-337.10029	-131
$TS3P_{vic\,(4,1)}$	-337.1135	-166	-337.094742	-117
$P_{vic\,(4,1)}$	-337.22397	-456	-337.192304	-373
$TSP_{vic}P_{dis\,(4,1)}$	-337.20507	-407	-337.175449	-329
$P_{dis\,(4,1)}$	-337.22438	-457	-337.205372	-407
$TSP_{gem}P_{vic\,(4,1)}$	-337.20852	-416	-337.17545	-329
$TS3P_{gem\,(4,1)}$	-337.09007	-105	-337.05264	-6
$P_{gem\,(4,1)}$	-337.22681	-464	-337.179527	-339

Table S4. Calculated NPA charges in electrons (e) of atoms within I3$_{(4,1)}$, TS3P$_{(4,1)vic}$ and P$_{(4,1)vic}$ in the doublet state.
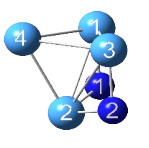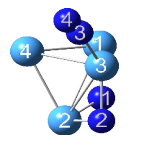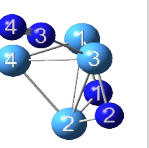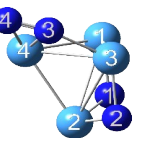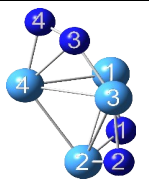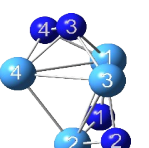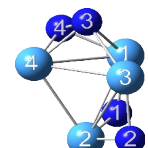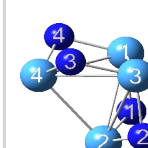
	I3$_{(4,1)}$	TS3P$_{(4,1)vic}$	P$_{(4,1)vic}$
Ta1	0.61512	0.60802	0.68992
Dif. *I3		-0.0071	0.0748
Dif. *TS3P$_{(4,1)vic}$			0.0819
Ta2	0.76117	0.85803	1.01663
Dif. *I3		0.09686	0.25546
Dif. *TS3P$_{(4,1)vic}$			0.1586
Ta3	0.67714	0.68491	0.69468
Dif. *I3		0.00777	0.01754
Dif. *TS3P$_{(4,1)vic}$			0.00977
Ta4	0.05111	0.04651	0.1791
Dif. *I3		-0.0046	0.12799
Dif. *TS3P$_{(4,1)vic}$			0.13259
N1	-0.57428	-0.64387	-0.78987
Dif. *I3		-0.06959	-0.21559
Dif. *TS3P$_{(4,1)vic}$			-0.146
N2	-0.53027	-0.5536	-0.79046

Table S5. Calculated energies of the cluster adsorbate complex $[Ta_4(N_2)_2]^+$ in the doublet state along the activation pathway of the second N_2 molecule depending on the adsorption site (Ta2, Ta3 or Ta4) to the $[Ta_4NN]^+$ cluster complex.
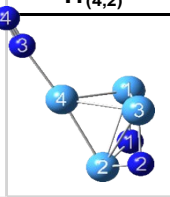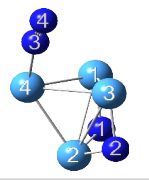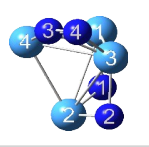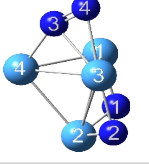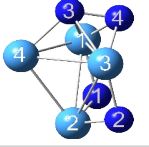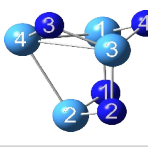
	N_2 adsorption on Ta3		N_2 adsorption on Ta4		N_2 adsorption on Ta2	
	energy E / Ha	ΔE / kJ/mol	energy E / Ha	ΔE / kJ/mol	energy E / Ha	ΔE / kJ/mol
$[Ta_4NN]^+$, N_2	-446.67025	0	-446.67025	0	-446.67025	0
I1$_{(4,2)}$	-446.68723	-45	-446.68591	-41	-446.69202	-57
TS12$_{(4,2)}$	-446.68534	-40	-446.67966	-25	-446.68012	-26
I2$_{(4,2)}$	-446.69788	-73	-446.70842	-100	-446.68996	-52
TS23$_{(4,2)}$	-446.67392	-10	-446.68283	-33	-446.64057	78
I3$_{(4,2)}$	-446.72388	-141	-446.73011	-157	-446.69561	-67
TS3P$_{(4,2)}$	-446.70106	-81	-446.71585	-120		
P$_{(4,2)}$	-446.80153	-345	-446.81452	-379		
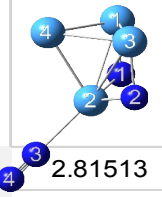
Table S6. Calculated distances in Å of atoms within [Ta$_4$NN]$^+$ (P$_{vic(4,1)}$), N$_2$ and [Ta$_4$(N$_2$)$_2$]$^+$ in the doublet state along the activation pathway of the second N$_2$ molecule on a [Ta$_4$NN]$^+$ cluster complex at the adsorption site Ta3.

	P$_{vic\,(4,1)}$	N$_2$	I1$_{(4,2)}$	TS12$_{(4,2)}$	I2$_{(4,2)}$	TS23$_{(4,2)}$	I3$_{(4,2)}$	TS3P$_{(4,2)}$	P$_{(4,2)}$
Ta1-Ta2	2.80981		2.82055	2.81846	2.81562	2.79044	2.84153	2.83419	2.86942
Ta2-Ta3	2.80852		2.81321	2.8097	2.83041	2.77281	2.7486	2.74203	2.86981
Ta3-Ta4	2.58246		2.58503	2.57503	2.62351	2.72479	2.61416	2.6479	2.86977
Ta1-Ta4	2.57679		2.56888	2.55941	2.61602	2.61317	2.9945	2.9591	2.86938
Ta2-Ta4	2.61516		2.63087	2.62885	2.66096	2.79316	2.7182	2.75419	2.75944
Ta1-Ta3	2.69019		2.71185	2.72558	2.73453	2.66141	2.65038	2.6742	2.75968
Ta1-N1	1.83777		1.83769	1.83437	1.83017	1.81963	1.86045	1.86293	1.87286
Ta1-N3							2.14574	2.31351	
Ta1-N4							1.98228	1.89827	1.87311
Ta2-N1	1.89471		1.89627	1.89915	1.90254	1.92068	1.90306	1.89545	1.87305
Ta2-N2	1.89543		1.88368	1.87654	1.88278	1.837	1.8778	1.87783	1.87285
Ta3-N2	1.83664		1.85651	1.86706	1.85636	1.92233	1.87172	1.87342	1.87306
Ta3-N3			2.30132	2.15797	2.06218	2.00033	2.1264	2.10443	1.87283
Ta4-N3					2.13317	2.1527	2.0368	1.88939	1.87309
Ta4-N4				3.37324	2.24011	1.96456	1.98694	2.02749	1.87284
N1-N2	2.97767		2.98932	2.98721	2.99665	3.06684	3.1244	3.10173	3.08235
N3-N4		1.08948	1.09618	1.11553	1.17958	1.26022	1.44534	1.86585	3.08214
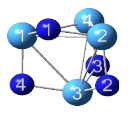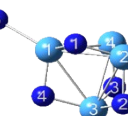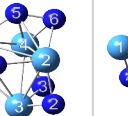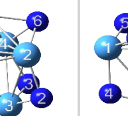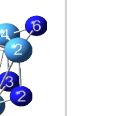
Table S7. Calculated distances in Å of atoms within [Ta$_4$NN]$^+$ (P$_{vic(4,1)}$), N$_2$ and [Ta$_4$(N$_2$)$_2$]$^+$ in the doublet state along the activation pathway of the second N$_2$ molecule on a [Ta$_4$NN]$^+$ cluster complex at the adsorption site Ta4.

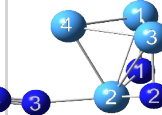|	P$_{vic(4,1)}$	N$_2$	I1$_{(4,2)}$	TS12$_{(4,2)}$	I2$_{(4,2)}$	TS23$_{(4,2)}$	I3$_{(4,2)}$	TS3P$_{(4,2)}$	P$_{(4,2)}$
Ta1-Ta2	2.80981		2.83727	2.81923	2.84027	2.79306	2.82791	2.83734	2.89667
Ta2-Ta3	2.80852		2.83709	2.81664	2.81509	2.77074	2.82787	2.81818	2.89051
Ta3-Ta4	2.58246		2.58158	2.58516	2.65604	2.66614	2.61228	2.62146	2.80618
Ta1-Ta4	2.57679		2.58141	2.5747	2.60394	2.57583	2.61193	2.67172	2.73099
Ta2-Ta4	2.61516		2.72586	2.69287	2.68509	2.71478	2.6901	2.7219	2.73246
Ta1-Ta3	2.69019		2.67366	2.68907	2.72829	2.73086	3.13204	3.03091	2.88981
Ta1-N1	1.83777		1.84822	1.84722	1.83673	1.821	1.86045	1.87169	1.87684
Ta1-N3							2.00934	2.26048	
Ta1-N4							2.16871	1.91141	1.85197
Ta2-N1	1.89471		1.88124	1.88215	1.8974	1.91623	1.88128	1.87141	1.87634
Ta2-N2	1.89543		1.88112	1.90161	1.86633	1.86	1.88118	1.86907	1.85192
Ta3-N2	1.83664		1.84818	1.83024	1.87476	1.89818	1.86052	1.87643	1.90732
Ta3-N3				2.78782	2.13583	2.16181	2.16863	2.17606	193905
Ta3-N4					2.13585	2.18539	2.00921	1.9844	1.90715
Ta4-N3			2.28513	2.14424	2.01852	1.94927	1.94453	1.85692	1.82058
N1-N2	2.97767		3.0311	3.02961	3.00888	2.98675	3.04954	3.01691	2.97204
N3-N4		1.08948	1.09805	1.1171	1.19908	1.22114	1.45082	1.88124	3.22509

Table S8. Calculated distances in Å of atoms within [Ta$_4$NN]$^+$ (P$_{vic(4,1)}$), N$_2$ and [Ta$_4$(N$_2$)$_2$]$^+$ in the doublet state along the activation pathway of the second N$_2$ molecule on a [Ta$_4$NN]$^+$ cluster complex at the adsorption site Ta2.

	P$_{vic(4,1)}$	N$_2$	I1$_{(4,2)}$	TS12$_{(4,2)}$	I2$_{(4,2)}$	TS23$_{(4,2)}$	I3$_{(4,2)}$
Ta1-Ta2	2.80981		2.81513	2.78882	2.79645	2.79156	2.80208
Ta2-Ta3	2.80852		2.81529	2.78883	2.79699	2.77467	2.6197
Ta3-Ta4	2.58246		2.58552	2.58659	2.63276	2.52906	2.95895
Ta1-Ta4	2.57679		2.58532	2.58658	2.63207	2.64573	2.582
Ta2-Ta4	2.61516		2.62512	2.62782	2.68194	2.65112	3.06341
Ta1-Ta3	2.69019		2.70673	2.70501	2.68166	2.7193	2.71683
Ta1-N1	1.83777		1.83311	1.83438	1.84518	1.8294	1.861
Ta2-N1	1.89471		1.90516	1.91897	1.9048	1.91194	1.88476
Ta2-N2	1.89543		1.90542	1.91897	1.90526	1.89714	1.9482
Ta2-N3			2.36296	2.14761	2.07339	2.19879	2.01995
Ta2-N4							2.39541
Ta3-N2	1.83664		1.83295	1.83437	1.84477	1.83515	1.83541
Ta3-N4							1.97752
Ta4-N3				2.60943	2.13529	2.13624	1.97593
Ta4-N4					2.2617	2.25311	2.01989
N1-N2	2.97767		3.01154	3.15922	3.19045	2.8922	3.14599
N3-N4		1.08948	1.09143	1.12419	1.18514	1.17595	1.43254

Table S9. Calculated distances in Å of atoms within [Ta$_4$NNNN]$^+$ (P$_{(4,2)}$), N$_2$ and [Ta$_4$(N$_2$)$_3$]$^+$ in the doublet state along the activation pathway of the third N$_2$ molecule on a [Ta$_4$NNNN]$^+$ cluster complex.

	P$_{(4,2)}$	N$_2$	I1$_{(4,3)}$	TS12$_{(4,3)}$	I2$_{(4,3)}$	TS23$_{(4,3)}$	I3$_{(4,3)}$	TS3P$_{(4,3)}$	P$_{(4,3)}$
Ta1-Ta2	2.89667		2.90994	2.87769	2.93005	2.85026	2.72582	2.76575	3.0643
Ta2-Ta3	2.89051		2.90311	2.92722	2.98695	3.01501	2.88929	2.86835	3.06265
Ta3-Ta4	2.80618		2.8047	2.82866	2.83734	2.94419	2.54255	2.57789	3.06413
Ta1-Ta4	2.73099		2.72676	2.71213	2.75695	2.67934	2.85667	2.9236	3.06575
Ta2-Ta4	2.73246		2.75834	2.76559	2.8308	2.75024	2.93891	2.89893	3.06486
Ta1-Ta3	2.88981		2.88935	2.83791	2.85544	3.05579	3.37458	3.38825	3.06333
Ta1-N1	1.87684		1.90147	1.906	1.90697	1.90828	1.83387	1.83147	1.88945
Ta1-N4	1.85197		1.85296	1.88849	1.87502	1.88057	1.97257	1.9503	1.8892
Ta1-N5			2.35714	2.18602	2.0513	2.18602	1.91426	1.89104	1.88959
Ta2-N1	1.87634		1.86135	1.86241	1.85264	1.85229	1.95201	1.96964	1.88959
Ta2-N2	1.85192		1.85731	1.85202	1.84419	1.85237	1.8486	1.85811	1.88944
Ta2-N5							2.34129	2.37533	
Ta2-N6							2.1297	2.04184	1.88967
Ta3-N2	1.90732		1.90617	1.9099	1.91809	1.89812	1.92122	1.91462	1.88953
Ta3-N3	193905		1.94295	1.94474	1.91172	1.87877	1.86091	1.85886	1.8894
Ta3-N4	1.90715		1.90975	1.89442	1.90933	1.88815	2.08733	2.04167	1.8898
Ta4-N3	1.82058		1.81801	1.81703	1.85547	1.88415	1.91334	1.91923	1.88949
Ta4-N5					2.1355	2.20318	2.16854	2.13948	1.88935
Ta4-N6					2.12976	2.20298	2.02923	1.94534	1.88927
N1-N2	2.97204		2.98615	2.99346	3.00743	2.7984	2.89833	2.94792	3.09657
N3-N4	3.22509		3.22173	3.23665	3.21198	3.09707	2.79033	2.79851	3.0969
N5-N6		1.08948	1.09095	1.11783	1.20694	1.2035	1.38899	1.86645	3.09568

Table S10. Calculated energies of the cluster adsorbate complex $[Ta_4(N_2)_3]^+$ in the doublet state along the activation pathway of the third N_2 molecule to the $[Ta_4NNNN]^+$ cluster complex.

	energy E / Ha	ΔE in kJ/mol
$[Ta_4NNNN]^+$, N_2	-556.2608	0
$I1_{(4,3)}$	-556.28521	-64
$TS12_{(4,3)}$	-556.26904	-22
$I2_{(4,3)}$	-556.29382	-87
$TS23_{(4,3)}$	-556.23984	55
$I3_{(4,3)}$	-556.28957	-76
$TS3P_{(4,3)}$	-556.25859	6
$P_{(4,3)}$	-556.35682	-252

Table S11. Calculated energies and vibrational frequencies of model systems (scaling factor: 0.9376).

	$Ta_4(N_2)_3^+$	$[Ta_4(N_2)_4]^+$				$[Ta_4(N_2)_5]^+$					
	$I2_{(4,3)}$	$(4,4)_{400}$ *Ta1	$(4,4)_{401}$ *Ta2	$(4,4)_{402}$ *Ta4	$(4,4)_{403}$ *Ta3	$(4,5)_{400}$ *Ta1 *Ta2	$(4,5)_{402}$ *Ta1 *Ta3	$(4,5)_{401}$ *Ta1 *Ta4	$(4,5)_{420}$ *Ta4 *Ta3	$(4,5)_{411}$ *Ta2 *Ta3	$(4,5)_{410}$ *Ta2 *Ta4
energy E / Ha	-556.29382	-665.76333	-665.76489	-665.76475	-665.76465	-775.2347	-775.23182	-775.23465	-775.23487	-775.23609	-775.23499
energy E / kJ/mol		-1747961.382	-1747965.478	-1747965.11	-1747964.848	-2035378.424	-2035370.863	-2035378.293	-2035378.871	-2035382.074	-2035379.186
$\nu_{(N5N6)}$ / cm^{-1}	1516.31	1473.52	1517.75	1490.68	1475.3	1474.1	1458.64	1423.29	1414.9	1478.16	1475.63
$\nu_{(N5N6)scal}$ / cm^{-1}	1422	1382	1423	1398	1383	1382	1368	1334	1327	1386	1384
$\nu_{(N7N8)}$ / cm^{-1}		2481.53	2461.79	2403.02	2492.59	2481.4	2480.81	2476.65	2406.97	2415	2476.27
$\nu_{(N7N8)scal}$ / cm^{-1}		2326.615362	2308.107672	2253.006511	2336.984918	2326.493477	2325.940309	2322.040006	2256.709924	2264.238634	2321.683728
$\nu_{(N9N10)}$ / cm^{-1}						2423.01	2491.86	2405.77	2488.26	2492.84	2399.66
$\nu_{(N9N10)scal}$ / cm^{-1}						2271.748594	2336.30049	2255.584836	2332.925228	2337.219312	2249.856266

22

Table S12. Calculated distances in Å of atoms within model systems in the doublet state.

	$Ta_4(N_2)_3^+$	$[Ta_4(N_2)_4]^+$				$[Ta_4(N_2)_5]^+$					
	$I2_{(4,3)}$	$(4,4)_{400}$ *Ta1	$(4,4)_{401}$ *Ta2	$(4,4)_{402}$ *Ta4	$(4,4)_{403}$ *Ta3	$(4,5)_{400}$ *Ta1 *Ta2	$(4,5)_{402}$ *Ta1 *Ta3	$(4,5)_{401}$ *Ta1 *Ta4	$(4,5)_{420}$ *Ta4 *Ta3	$(4,5)_{411}$ *Ta2 *Ta3	$(4,5)_{410}$ *Ta2 *Ta4
Ta1-Ta2	2.93005	2.96352	2.9226	2.93769	2.91401	2.94426	2.92393	2.97832	2.92776	2.88943	2.93332
Ta2-Ta3	2.98695	2.9486	2.976	2.97279	3.02814	2.92539	2.98623	2.93948	3.02048	3.00167	2.96424
Ta3-Ta4	2.83734	2.80566	2.84709	2.87449	2.88121	2.83583	2.87097	2.83913	2.91576	2.90965	2.88324
Ta1-Ta4	2.75695	2.80731	2.77777	2.81097	2.73511	2.82968	2.77981	2.83961	2.78023	2.76349	2.8256
Ta2-Ta4	2.8308	2.81436	2.83143	2.85005	2.82047	2.80704	2.78142	2.81862	2.82894	2.81037	2.85432
Ta1-Ta3	2.85544	2.89859	2.86735	2.84297	2.89649	2.93278	2.95135	2.92159	2.9092	2.93339	2.85337
Ta1-N1	1.90697	1.91016	1.9046	1.90687	1.91042	1.90379	1.91529	1.90849	1.91203	1.90209	1.90545
Ta1-N4	1.87502	1.87323	1.87602	1.87158	1.88034	1.87555	1.87698	1.87425	1.88098	1.88406	1.87392
Ta1-N5	2.0513	2.03829	2.05057	2.05122	2.04029	2.0344	2.031	2.03136	2.02038	2.03581	2.04593
Ta1-N7		2.3757				2.37482	2.39362	2.36477			
Ta2-N1	1.85264	1.85783	1.86394	1.85562	1.85238	1.87465	1.85735	1.86201	1.85336	1.87002	1.8647
Ta2-N2	1.84419	1.84845	1.8562	1.84425	1.8521	1.86459	1.86124	1.84785	1.85194	1.87132	1.8522
Ta2-N7			2.37603							2.32757	2.39398
Ta2-N9						2.33544					
Ta3-N2	1.91809	1.91638	1.91333	1.91986	1.91584	1.90728	1.90737	1.91846	1.91658	1.90478	1.9186
Ta3-N3	1.91172	1.91774	1.91408	1.91217	1.90912	1.91959	1.91035	1.91568	1.9078	1.91285	1.91335
Ta3-N4	1.90933	1.91615	1.91261	1.91253	1.91061	1.9165	1.91806	1.91141	1.90751	1.90943	1.91301
Ta3-N7					2.38548						
Ta3-N9						2.39766			2.38438	2.3876	
Ta4-N3	1.85547	1.8532	1.85431	1.85345	1.86258	1.85038	1.86262	1.8541	1.86273	1.85856	1.85403
Ta4-N5	2.1355	2.12958	2.13941	2.1306	2.11912	2.13757	2.1166	2.122	2.10771	2.12673	2.13181
Ta4-N6	2.12976	2.12091	2.1243	2.17063	2.10878	2.11489	2.10592	2.16231	2.143	2.10529	2.16701
Ta4-N7				2.2843					2.28743		
Ta4-N9						2.28335					2.28658
N5-N6	1.20694	1.21471	1.20768	1.20584	1.21869	1.21592	1.22442	1.21875	1.22772	1.21933	1.20793
N7-N8		1.08882	1.8956	1.09306	1.08829	1.08882	1.08881	1.08908	1.09308	1.09223	1.08903
N9-N10						1.09173	1.08817	1.09311	1.08834	1.08818	1.09319

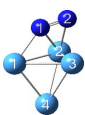**Table S13.** Calculated NPA charges in electrons (e) of atoms within model systems in the doublet state.

	$[Ta_3(N_2)_4]^+$	$[Ta_4(N_2)_4]^+$				$[Ta_4(N_2)_5]^+$					
	I2$_{(4,3)}$	(4,4)$_{400}$ *Ta1	(4,4)$_{401}$ *Ta2	(4,4)$_{402}$ *Ta4	(4,4)$_{403}$ *Ta3	(4,5)$_{400}$ *Ta1 *Ta2	(4,5)$_{402}$ *Ta1 *Ta3	(4,5)$_{401}$ *Ta1 *Ta4	(4,5)$_{420}$ *Ta4 *Ta3	(4,5)$_{411}$ *Ta2 *Ta3	(4,5)$_{410}$ *Ta2 *Ta4
	npa	npa	npa	npa	npa	npa	npa	npa	npa	npa	npa
Ta1	1.516	1.444	1.527	1.532	1.507	1.458	1.445	1.468	1.544	1.534	1.538
Ta2	1.336	1.321	1.209	1.34	1.324	1.182	1.295	1.328	1.33	1.19	1.221
Ta4	1.069	1.096	1.093	0.963	1.086	1.133	1.092	0.978	0.999	1.123	0.986
Ta3	1.757	1.721	1.757	1.735	1.677	1.738	1.668	1.726	1.676	1.686	1.732
N4	-1.022	-1.02	-1.028	-1.017	-1.022	-1.027	-1.024	-1.017	-1.021	-1.031	-1.023
N3	-1.003	-0.999	-1.007	-0.988	-1.001	-1.003	-0.998	-0.985	-0.988	-1.004	-0.991
N2	-1.014	-1.015	-1.019	-1.013	-1.021	-1.021	-1.022	-1.016	-1.02	-1.026	-1.017
N1	-0.988	-0.995	-0.996	-0.996	-0.991	-1.001	-0.994	-1.002	-0.999	-0.999	-1.002
N5	-0.426	-0.435	-0.428	-0.433	-0.451	-0.438	-0.455	-0.455	-0.486	-0.454	-0.437
N6	-0.224	-0.247	-0.23	-0.207	-0.251	-0.256	-0.267	-0.241	-0.257	-0.256	-0.218
N7		-0.105	-0.118	-0.123	-0.103	-0.102	-0.098	-0.101	-0.114	-0.125	-0.11
N8		0.235	0.242	0.204	0.244	0.233	0.222	0.232	0.196	0.222	0.24
N9						-0.121	-0.1	-0.114	-0.1	-0.103	-0.117
N10						0.225	0.237	0.199	0.241	0.244	0.198

24

Table S14. Total energies of the activation pathway of the first N_2 molecule in the doublet state from I2 to P_{vic} by DFT with various functionals. These values are visualized in Fig. S8.

		$I2_{(4,1)}$	$TS23_{(4,1)}$	$I3_{(4,1)}$	$TS3P_{vic\,(4,1)}$	$P_{vic\,(4,1)}$
B3LYP	energy E / Ha	-337.320685	-337.292027	-337.332639	-337.331014	-337.448346
	ΔE / kJ/mol	0.000000	75.241579	-31.385227	-27.118789	-335.173955
PBE	energy E / Ha	-337.345128	-337.318768	-337.356264	-337.355091	-337.459392
	ΔE / kJ/mol	0.000000	69.208180	-29.237568	-26.157857	-300.000132
M06	energy E / Ha	-337.094349	-337.067648	-337.109171	-337.104272	-337.220527
	ΔE / kJ/mol	0.000000	70.103476	-38.915161	-26.052836	-331.280339
TPSSh	energy E / Ha	-337.266114	-337.243832	-337.285250	-337.284140	-337.391540
	ΔE / kJ/mol	0.000000	58.501391	-50.241568	-47.327263	-329.305963
PBE0	energy E / Ha	-337.095144	-337.072693	-337.117157	-337.113500	-337.223969
	ΔE / kJ/mol	0.000000	58.945100	-57.795132	-48.193678	-338.230038
riCC2	energy E / Ha	-336.227918	-336.213484	-336.246759		
	ΔE / kJ/mol	0.000000	37.896118	-49.467877		

Table S15. Calculated distances in Å of atoms within in the doublet state along the activation pathway of the first N_2 molecule from $I2_{(4,1)}$ to $P_{vic(4,1)}$.

	B3LYP					PBE					M06				
	$I2_{(4,1)}$	$TS23_{(4,1)}$	$I3_{(4,1)}$	$TS3P_{vic(4,1)}$	$P_{vic(4,1)}$	$I2_{(4,1)}$	$TS23_{(4,1)}$	$I3_{(4,1)}$	$TS3P_{vic(4,1)}$	$P_{vic(4,1)}$	$I2_{(4,1)}$	$TS23_{(4,1)}$	$I3_{(4,1)}$	$TS3P_{vic(4,1)}$	$P_{vic(4,1)}$
Ta1-Ta2	2.65984	2.63563	2.97672	3.02459	2.84429	2.65862	2.59166	2.97877	3.01261	2.82649	2.65692	2.6092	2.95716	2.99994	2.82557
Ta2-Ta3	2.59167	2.45614	2.90466	2.85321	2.84454	2.5881	2.44783	2.88381	2.83954	2.82677	2.59247	2.45758	2.8774	2.81735	2.82581
Ta3-Ta4	2.62905	2.8013	2.56689	2.57968	2.60001	2.61793	2.55439	2.55891	2.56915	2.59076	2.62944	2.56406	2.56521	2.57954	2.6024
Ta1-Ta4	2.58104	2.5907	2.5904	2.59877	2.59902	2.58246	2.5921	2.57583	2.58239	2.58962	2.58096	2.60473	2.58755	2.593	2.60213
Ta2-Ta4	2.59164	2.5786	2.48043	2.46998	2.64218	2.58799	2.78616	2.47428	2.46988	2.6206	2.59237	2.77211	2.4764	2.47438	2.63388
Ta1-Ta3	2.58115	2.60688	2.5343	2.53295	2.72281	2.58259	2.61781	2.52506	2.52819	2.71311	2.58101	2.61794	2.52864	2.53773	2.72331
Ta1-N1	2.04537	2.04236	1.92841	1.92436	1.85094	2.02556	2.05497	1.94026	1.93317	1.85581	2.04112	2.02827	1.92427	1.90896	1.83591
Ta1-N2															
Ta2-N1	2.15814	2.35143	2.23764	2.15198	1.90701	2.15173	2.23917	2.22235	2.15608	1.9148	2.135	2.18804	2.20343	2.11612	1.8977
Ta2-N2	2.21616	2.42092	1.97115	1.93923	1.9078	2.1951	2.15171	1.96937	1.94022	1.91558	2.19197	2.12912	1.95865	1.91728	1.89802
Ta3-N1			2.23483	2.31594				2.23401	2.30126				2.21046	2.30258	
Ta3-N2			2.01518	1.96782	1.85043			2.02674	1.97954	1.85534			2.00475	1.94323	1.83568
N1-N2	1.18745	1.24672	1.454	1.6375		1.20733	1.25761	1.46239	1.63096		1.18614	1.24254	1.43319	1.69166	

Table S16. Calculated distances in Å of atoms within in the doublet state along the activation pathway of the first N_2 molecule from $I2_{(4,1)}$ to $P_{vic(4,1)}$.

	TPSSh					riCC2		
	$I2_{(4,1)}$	$TS23_{(4,1)}$	$I3_{(4,1)}$	$TS3P_{vic(4,1)}$	$P_{vic(4,1)}$	$I2_{(4,1)}$	$TS23_{(4,1)}$	$I3_{(4,1)}$
Ta1-Ta2	2.65011	2.59638	2.94698	2.99392	2.81875	2.60103	2.57941	2.95411
Ta2-Ta3	2.58543	2.47599	2.87627	2.82788	2.81888	2.54261	2.3976	2.79764
Ta3-Ta4	2.61885	2.52904	2.55728	2.56923	2.58887	2.7015	2.64785	2.50717
Ta1-Ta4	2.5768	2.60134	2.57374	2.58095	2.58859	2.5709	2.60455	2.56382
Ta2-Ta4	2.58532	2.77862	2.47722	2.46714	2.63041	2.54215	2.57809	2.41448
Ta1-Ta3	2.57707	2.60288	2.5224	2.5205	2.7055	2.55912	2.64278	2.53324
Ta1-N1	2.02394	2.04654	1.93295	1.9298	1.85178	2.02402	2.22505	2.01614
Ta1-N2								
Ta2-N1	2.13369	2.18569	2.20682	2.14083	1.90694	2.1085	2.27548	2.23521
Ta2-N2	2.18297	2.12726	1.9678	1.94123	1.90725	2.08954	2.20161	1.95075
Ta3-N1			2.21589	2.28349				2.24771
Ta3-N2			2.01536	1.97124	1.85143			2.09205
Ta4-N1								
N1-N2	1.2009	1.23751	1.46539	1.62748		1.23047	1.1583	1.48957

27

SI References

1. C. Berg, T. Schindler, G. Niedner-Schatteburg and V. E. Bondybey, *J. Chem. Phys.*, 1995, **102**, 4870-4884.
2. V. E. Bondybey and J. H. English, *J. Chem. Phys.*, 1981, **74**, 6978-6979.
3. D. Proch and T. Trickl, *Rev. Sci. Instrum.*, 1989, **60**, 713-716.
4. P. Caravatti and M. Allemann, *Org Mass Spectrom*, 1991, **26**, 514-518.
5. M. Graf, Diploma Technische Universität Kaiserslautern, 2006.
6. T. Su and M. T. Bowers, *International Journal of Mass Spectrometry and Ion Physics*, 1973, **12**, 347-356.
7. I. Balteanu, O. P. Balaj, B. S. Fox-Beyer, P. Rodrigues, M. T. Barros, A. M. C. Moutinho, M. L. Costa, M. K. Beyer and V. E. Bondybey, *Organometallics*, 2004, **23**, 1978-1985.
8. G. Kummerlöwe and M. K. Beyer, *International Journal of Mass Spectrometry*, 2005, **244**, 84-90.
9. M. J. Frisch, G. W. Trucks, H. B. Schlegel, G. E. Scuseria, M. A. Robb, J. R. Cheeseman, G. Scalmani, V. Barone, B. Mennucci, G. A. Petersson, H. Nakatsuji, M. Caricato, X. Li, H. P. Hratchian, A. F. Izmaylov, J. Bloino, G. Zheng, J. L. Sonnenberg, M. Hada, M. Ehara, K. Toyota, R. Fukuda, J. Hasegawa, M. Ishida, T. Nakajima, Y. Honda, O. Kitao, H. Nakai, T. Vreven, J. A. Montgomery Jr., J. E. Peralta, F. Ogliaro, M. J. Bearpark, J. Heyd, E. N. Brothers, K. N. Kudin, V. N. Staroverov, R. Kobayashi, J. Normand, K. Raghavachari, A. P. Rendell, J. C. Burant, S. S. Iyengar, J. Tomasi, M. Cossi, N. Rega, N. J. Millam, M. Klene, J. E. Knox, J. B. Cross, V. Bakken, C. Adamo, J. Jaramillo, R. Gomperts, R. E. Stratmann, O. Yazyev, A. J. Austin, R. Cammi, C. Pomelli, J. W. Ochterski, R. L. Martin, K. Morokuma, V. G. Zakrzewski, G. A. Voth, P. Salvador, J. J. Dannenberg, S. Dapprich, A. D. Daniels, Ö. Farkas, J. B. Foresman, J. V. Ortiz, J. Cioslowski and D. J. Fox, Gaussian 09, Revision D.01, Gaussian, Inc., Wallingford, CT, USA, 2009.
10. M. J. Frisch, G. W. Trucks, H. B. Schlegel, G. E. Scuseria, M. A. Robb, J. R. Cheeseman, G. Scalmani, V. Barone, G. A. Petersson, H. Nakatsuji, X. Li, M. Caricato, A. V. Marenich, J. Bloino, B. G. Janesko, R. Gomperts, B. Mennucci, H. P. Hratchian, J. V. Ortiz, A. F. Izmaylov, J. L. Sonnenberg, Williams, F. Ding, F. Lipparini, F. Egidi, J. Goings, B. Peng, A. Petrone, T. Henderson, D. Ranasinghe, V. G. Zakrzewski, J. Gao, N. Rega, G. Zheng, W. Liang, M. Hada, M. Ehara, K. Toyota, R. Fukuda, J. Hasegawa, M. Ishida, T. Nakajima, Y. Honda, O. Kitao, H. Nakai, T. Vreven, K. Throssell, J. A. Montgomery Jr., J. E. Peralta, F. Ogliaro, M. J. Bearpark, J. J. Heyd, E. N. Brothers, K. N. Kudin, V. N. Staroverov, T. A. Keith, R. Kobayashi, J. Normand, K. Raghavachari, A. P. Rendell, J. C. Burant, S. S. Iyengar, J. Tomasi, M. Cossi, J. M. Millam, M. Klene, C. Adamo, R. Cammi, J. W. Ochterski, R. L. Martin, K. Morokuma, O. Farkas, J. B. Foresman and D. J. Fox, Gaussian 16, Revision C.01, Gaussian, Inc., Wallingford, CT, USA, 2016.
11. J. P. Perdew, K. Burke and M. Ernzerhof, *Phys. Rev. Lett.*, 1996, **77**, 3865-3868.
12. C. Adamo and V. Barone, *J. Chem. Phys.*, 1999, **110**, 6158-6170.
13. F. Weigend and R. Ahlrichs, *PCCP*, 2005, **7**, 3297-3305.

14.   D. Andrae, U. Häußermann, M. Dolg, H. Stoll and H. Preuß, *Theoretica Chimica Acta*, 1990, **77**, 123-141.
15.   M. P. Klein, A. A. Ehrhard, J. Mohrbach, S. Dillinger and G. Niedner-Schatteburg, *Topics in Catalysis*, 2018, **61**, 106-118.
16.   J. Mohrbach, S. Dillinger and G. Niedner-Schatteburg, *The Journal of Physical Chemistry C*, 2017, **121**, 10907-10918.
17.   S. Dillinger, M. P. Klein, A. Steiner, D. C. McDonald, M. A. Duncan, M. M. Kappes and G. Niedner-Schatteburg, *The Journal of Physical Chemistry Letters*, 2018, **9**, 914-918.
18.   C. Peng and H. Bernhard Schlegel, 1993, **33**, 449-454.
19.   L. Fan, D. Harrison, L. Deng, T. K. Woo, D. Swerhone and T. Ziegler, *Can. J. Chem.*, 1995, **73**, 989-998.
20.   K. Fukui, *Acc. Chem. Res.*, 1981, **14**, 363-368.
21.   F. Weinhold and J. E. Carpenter, in *The Structure of Small Molecules and Ions*, eds. R. Naaman and Z. Vager, Springer US, Boston, MA, 1988, DOI: 10.1007/978-1-4684-7424-4_24, pp. 227-236.
22.   E. D. Glendening, C. R. Landis and F. Weinhold, 2013, **34**, 1429-1437.
23.   T. A. Albright, J. K. Burdett and M. H. Whangbo, in *Orbital Interactions in Chemistry*, eds. T. A. Albright, J. K. Burdett and M. H. Whangbo, John Wiley & Sons, 2013, DOI: 10.1002/9781118558409.ch18, ch. 18, pp. 503-526.
24.   M. D. Fryzuk, S. A. Johnson and S. J. Rettig, *J. Am. Chem. Soc.*, 1998, **120**, 11024-11025.
25.   M. Zhou, X. Jin, Y. Gong and J. Li, *Angew. Chem. Int. Ed.*, 2007, **46**, 2911-2914.
26.   Y. Gong, Zhao and M. Zhou, *J. Phys. Chem. A*, 2007, **111**, 6204-6207.
27.   X. Cheng, Z.-Y. Li, L.-H. Mou, Y. Ren, Q.-Y. Liu, X.-L. Ding and S.-G. He, *Chemistry - A European Journal*, 2019, **25**, 16523-16527.
28.   M. D. Fryzuk, S. A. Johnson, B. O. Patrick, A. Albinati, S. A. Mason and T. F. Koetzle, *J. Am. Chem. Soc.*, 2001, **123**, 3960-3973.